

A mathematical model for top-shelf vertigo: the role of sedimenting otoconia in BPPV

Todd M. Squires¹, Michael S. Weidman², Timothy C. Hain³ and Howard A. Stone²

¹*Departments of Applied and Computational Mathematics and Physics,
California Institute of Technology, Pasadena, CA 91125*

²*Division of Engineering and Applied Sciences, Harvard University, Cambridge, MA 02138*

³*Northwestern University Medical School, Chicago, IL 60611*

(Dated: December 13, 2018)

Benign Paroxysmal Positional Vertigo (BPPV) is a mechanical disorder of the vestibular system, in which calcite particles called otoconia interfere with the mechanical functioning of the fluid-filled semicircular canals normally used to sense rotation. Using hydrodynamic models, we examine the two mechanisms proposed by the medical community for BPPV: cupulolithiasis, in which otoconia attach directly to the cupula (a sensory membrane), and canalithiasis, in which otoconia settle through the canals and exert a fluid pressure across the cupula. Extending known hydrodynamic calculations and making reasonable geometric and physical approximations, we derive an expression for the transcupular pressure ΔP_c exerted by a settling solid particle in canalithiasis. By tracking settling otoconia in a model two-dimensional geometry, the cupular displacement and associated eye response (nystagmus) can be calculated quantitatively. Several important features emerge: 1) A pressure amplification occurs as otoconia enter a narrowing duct (almost twenty-fold in humans); 2) An average-sized otoconium requires approximately five seconds to settle through the wide ampulla, where ΔP_c is not amplified, which suggests a mechanism for the observed latency of BPPV; and 3) An average-sized otoconium can cause a volumetric cupular displacement on the order of 30 pL, corresponding to a step increase in angular velocity of $2^\circ/\text{s}$, approximately the threshold for sensation. Larger cupular displacement and nystagmus could result from larger and/or multiple otoconia.

I. INTRODUCTION

Benign Paroxysmal Positional Vertigo (BPPV) is the most commonly diagnosed vertigo syndrome [1], with a recent study suggesting that it affects 9% of older persons [2]. BPPV is characterized by sudden attacks of dizziness and nausea triggered by changes in head orientation, and specifically afflicts the posterior canal responsible for sensing ‘forward rolling’ rotations. The disorder has earned the common name “top-shelf vertigo”, since attacks often occur when the head is suddenly tilted back, such as when looking at objects on the top shelf. Other clinical features of BPPV include a 5-10 second *latency* between the head tilt and the onset of vertigo, and a *fatiguable* response which lessens with repeated head maneuvers [3]. Although the condition is not life-threatening, the disorientation brought on by attacks is severely discomforting, and can cause nausea, accidents and injuries.

BPPV is caused by a mechanical dysfunction of the vestibular system in the inner ear, whose fluid-filled *semicircular canals* normally act to detect angular rotation via deflections of the sensory membranous *cupula*. In BPPV, calcite particles (otoconia) are believed to interfere with the normal operation of the semicircular canals, falsely inducing a spinning sensation when in fact no rotary motion of the head is actually occurring.

Two primary theories for the cause of BPPV have been advanced by the medical community: *cupulolithiasis*, in which otoconia are directly attached to the cupula, and *canalithiasis*, in which otoconia freely sediment through the canals and exert a fluid pressure on the cupula. A consensus is emerging that canalithiasis is the more likely mechanism for BPPV, supported in part by the largely successful clinical technique used to treat BPPV treatment: therapeutic head maneuvers [4, 5, 6] designed to drive otoconia all the way around and out of the canal, so that they settle in the utricle. Further support for canalithiasis is reviewed in the work of Brandt and Steddin [3], who compare the two mechanisms and conclude that canalithiasis is better able to explain the latency and fatigability of the disorder. Recently, however, Buckingham [7] questioned the canalithiasis interpretation for the maneuvers, suggesting that settling particles should exert a transcupular pressure from the utricle as well as from the narrow duct. Finally, House and Honrubia [8] cite various clinical observations, some of which are consistent with canalithiasis, and some with cupulolithiasis, and suggest that in fact both mechanisms are viable.

Despite extensive quantitative modelling of normal vestibular functioning, the description and debate on BPPV mechanisms have been purely qualitative. Without a quantitative analysis of these mechanisms, it is impossible to know whether either mechanism is physically capable of producing a response of the magnitude experienced in BPPV. Very recently, House and Honrubia [8] have taken an important first step toward a quantitative mathematical model of canalithiasis and cupulolithiasis. Specifically, their canalithiasis model predicts that a settling sphere exerts a

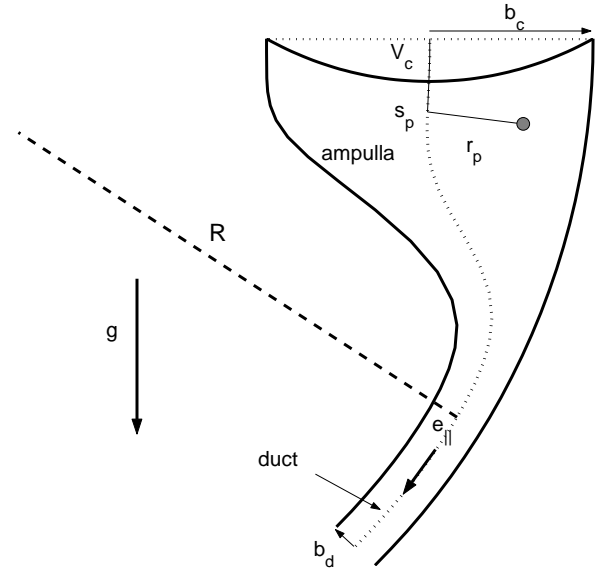
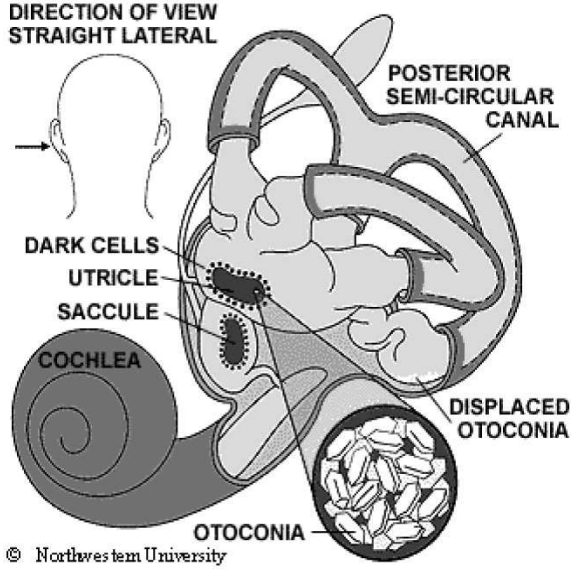


FIG. 1: a) The human vestibular system consists of the semicircular canals for sensing rotation, the otolithic organs (saccule and utricle) for sensing linear/gravitational acceleration, and the cochlea for auditory sensing. Displaced otoconia, perhaps from the otolithic organs, are believed to collect in the posterior canal and cause BPPV. b) Schematic of the model geometry for the semicircular canals (defined in equation 21), which is chosen to resemble measurements [9]. A torus of major radius R consists of a thin circular duct of radius b_d , and a thicker region consisting of the ampulla and the utricle (located above the cupula, not shown here). The ampulla and utricle are spanned and separated by the membranous cupula of radius b_c . The position of a sedimenting otoconium is specified by its distance s_p along the centerline of the canal and its distance r_p from the centerline of the canal. The translating otoconium exerts a pressure field that displaces the cupula by a volume V_c .

transcupular pressure (see, however, equation 11 below for the hydrodynamically correct result)

$$\Delta P_H = \frac{1}{3} \frac{F_{\parallel}}{A}, \quad (1)$$

where F_{\parallel} is the component of the buoyant force oriented along the axis of the canal, and A is the cross-sectional area of the canal at the location of the settling particle. This formula was argued intuitively based upon the following assumptions: the component of the force perpendicular to the channels exerts no transcupular pressure; only the drag on the sphere resulting from the pressure distribution contributes to the transcupular pressure; and the fluid pressure is uniform across each cross-section of the canal. A further assumption (not explicitly stated) is that the canal walls do not affect Stokes' law for a settling sphere, so that the Stokes settling velocity and pressure drag for a sphere settling in free space are used. While, strictly speaking, these assumptions are known to be incorrect, House and Honrubia correctly predict three key features of canalithiasis: (1) the characteristic magnitude of the transcupular pressure, (2) the amplification of transcupular pressure when the particle enters a narrow section of the channel, and (3) the inability of a force perpendicular to canal walls to result in a transcupular pressure.

The present work builds on and extends the results of House and Honrubia in several ways. First, we explicitly calculate the transcupular pressure resulting from a small particle settling through a fluid-filled channel using reasonable geometrical approximations. Significantly, both qualitative and quantitative corrections to equation (1) exist. Our expression is quantitatively accurate, is independent of particle shape or even size (so long as the particle is small compared to the channel), and is valid for a canal of arbitrary (but slowly-varying) geometry. Like equation (1), we provide a quantitative measure of forcing due to canalithiasis without requiring a detailed solution of the complete fluid equations in a complicated, three-dimensional geometry. Second, we consider two-dimensional motion of the otoconia (*i.e.* head maneuvers which are in the plane of the canal), so that otoconia settle out of the middle of the canal towards canal walls. We simulate BPPV episodes by tracking cupular displacement due to transcupular pressure ΔP_c , and (using a model of central 'velocity storage' that allows for additional processing by the brain stem) the nystagmus response \dot{E} . We compare this to a model of cupulolithiasis, and demonstrate that the former can actually give a *stronger* nystagmus response, as found by House and Honrubia.

This article is organized as follows: In sections II A and II B, respectively, we describe the normal functioning of the semicircular canals and mathematical models to describe it. In section III, we present the mathematical model

Physical parameters for human semicircular canals			
R	Major radius of semicircular canal	3.2 mm	from Curthoys and Oman [9]
b_d	Duct radius	0.16 mm	"
b_c	Mean radius of cupular partition	0.68 mm	"
δ	Angle over which channel tapers	.03 π	"
β_d	Angle subtended by duct	150°	Van Buskirk <i>et al.</i> [10]
β_u	Angle subtended by utricle	75°	"
ρ	Endolymph density	1.0 g/cm ³	Bronzino [13]
μ	Endolymph viscosity	.01 g/cm/s	"
ρ_o	Otoconium density	2.7 g/cm ³	"
a	Otoconium radius	0.5–15 μ m, 7.5 μ m avg.	Campos [14]
τ_c	Cupular time constant	4.2 s	Dai <i>et al.</i> [15]
τ_v	Nystagmus time constant	21 s	Malcolm [16]
K	Cupular elastic constant	13 GPa/m ³	Calculated using τ_c in (3)

TABLE I: Physical parameters and derived quantities for BPPV.

for canalithiasis based on the hydrodynamics of a settling particle, giving the resulting cupular response and, using a *velocity storage* model of neural processing, the measurable nystagmus response. Two-dimensional simulations of BPPV are provided in Section IV for two geometries: first, we treat a particle settling in a straight, tapering channel to demonstrate the geometric pressure amplification; second, we simulate an attack of BPPV in a model semicircular canal. The influence of otoconium size upon canalithiasis is discussed in Section V, and a model of cupulolithiasis is presented for comparison in Section VI. Finally, a summary is provided in Section VII, where the main results of this study are discussed.

II. THE SEMICIRCULAR CANALS: NORMAL FUNCTIONING AND MODELLING

A. Overview of normal vestibular functioning

The human vestibular system consists of two sets of organs: the otolithic organs, which sense linear acceleration and gravity, and the semicircular canals, which sense angular velocity and acceleration. Each ear has three semicircular canals that are oriented in a mutually orthogonal fashion in order to sense rotations about each of three axes, as shown in figure 1a. The canals are filled with endolymph of density ρ and viscosity μ similar to that of water.

Figure 1b depicts a model semicircular canal of major radius R which consists of the *duct*, which is a narrow region of radius b_d subtending an angle β_d , and a thicker region containing the *ampulla* and the *utricle* (spanning an angle β_u), which are in turn separated by the membranous cupula of radius b_c . We use β_d and β_u (not shown in the figure) to be consistent with the geometry of Van Buskirk *et al.* [10]. The figure, though somewhat simplified from the actual geometry, captures the most important shape variations, at least from the standpoint of the hydrodynamic analysis given in this paper. Typical geometric and material parameters are given in Table I.

When the canal experiences an angular acceleration, inertia causes the endolymph to lag behind the motion of the canal itself, distorting the cupula. The cupular distortion triggers embedded sensory hair cells to fire, signalling the angular acceleration/velocity to the brain and triggering a compensatory eye motion called *nystagmus*. Finally, the restoring force of the cupula pushes the endolymph back through the canal, and the cupula slowly relaxes to an undisplaced position.

Neural signal processing in the brain stem modifies the transmitted signal in a process called *velocity storage* [11, 12], lengthening the typical time constant of the associated sensation and nystagmus. The typical time constant for cupular relaxation ($\tau_c \approx 4$ s) is transformed into a nystagmus time constant of about $\tau_v \approx 21$ s for yaw (side-to-side) rotations, where the lateral semicircular canal is stimulated. Velocity storage may be less effective in the posterior canal, or might also be less effective for an unnatural vestibular stimulation such as BPPV. Nevertheless, since experimental data regarding the degree to which velocity storage applies in the posterior canal (indicated in Figure 1a) is presently unavailable, we assume that the same velocity storage is present as in the well-known situation with the lateral canals.

B. Mathematical models of the mechanics of semicircular canals

Steinhausen [17] developed the first model of the mechanics of the semicircular canals, treating the angular displacement $\theta(t)$ of the endolymph/cupula as an overdamped torsional pendulum, obeying the ordinary differential equation

$$I\ddot{\theta} + B\dot{\theta} + K\theta = -I\alpha, \quad (2)$$

where I reflects the inertia of the endolymph, B reflects viscous damping, K is the ‘spring constant’ of the elastic cupula, $\alpha(t)$ is the angular acceleration of the system, and overdots denote time derivatives. In this description, the response of the canals to stimuli is characterized by two time constants: (i) a long time scale $T_1 \approx B/K$, representing the relaxation time of a displaced cupula, which arises from a balance of the cupula’s restoring force against the viscous resistance of the duct to the fluid pushed through it; and (ii) a short time scale $T_2 \approx I/B$, representing the time over which the endolymphatic fluid moves inertially, which arises from a balance of inertia against viscous resistance.

Subsequent theoretical papers have attempted to calculate these time constants T_1 and T_2 from the physical parameters and length scales characteristic of the vestibular system. Van Buskirk, Watts and Liu [10] modelled a semicircular canal as a torus with thin (duct) and thick (utricle) sections. Neglecting the fluid flow in the utricle, and considering both transient and quasi-steady fluid flow through the duct, Van Buskirk *et al.* confirmed that the semicircular canals respond like an overdamped harmonic oscillator, and explicitly calculated the time constants in terms of system dimensions and parameters,

$$T_1 = \frac{8\mu\beta_d R}{\pi b_d^4 K} \quad \text{and} \quad T_2 = \frac{\rho b_d^2}{\lambda_1^2 \mu}, \quad (3)$$

where λ is the first zero of the Bessel function $J_0(\lambda)$. In response to a step increase in angular velocity $\alpha(t) = \Omega_0 \delta(t)$, the endolymph in the duct attains a maximum displacement of angle $\theta_m \approx 4\rho\Omega_0(1 + \beta_u/\beta_d)b_d^2/\lambda_1^4\mu$ after a time of approximately T_2 . This response corresponds to a maximum cupular displacement of volume

$$V_c \approx \theta_m R \pi b_d^2 = \frac{4\rho\Omega_0(1 + \beta_u/\beta_d)\pi R b_d^4}{\lambda_1^4 \mu}, \quad (4)$$

which decays back to zero on a time scale T_1 .

Equation (4) provides a convenient way to compare the cupular displacement due to a settling otoconium to that driven by an equivalent rotation Ω . Using values from Table I, the volumetric cupular displacement V_0 corresponding to the measured detection threshold ($\Omega_c \approx 2^\circ/\text{s}$) is approximately $V_0 \approx 35 \text{ pL}$.

In this approach, all physical and geometrical parameters are known except for the cupular stiffness K , which Van Buskirk *et al.* assumed to be $K = 3.4 \text{ GPa/m}^3$ in order to obtain a long time constant $T_1 = 21 \text{ s}$, as found in nystagmus measurements by Malcolm [16]. This assumption is now known to be likely in error, as nystagmus is believed to reflect a neural signal processed by the so-called ‘velocity storage mechanism’ [11, 12], as discussed shortly. The human cupular time constant is believed to be approximately 4.2 s [18], which yields a corresponding cupular stiffness constant $K \approx 13 \text{ GPa/m}^3$.

Revisions to the approach of Van Buskirk *et al.* include the work of Oman, Marcus and Curthoys [19], who considered a more realistic description of the semicircular canals, using geometries that did not have constant, circular cross-section, and Rabbitt and Damiano [20] who accounted for vestibular functioning at high accelerations by calculating the fluid flow near the cupula partition rather than assuming a Poiseuille profile. Furthermore, Damiano [21] allowed for fluid to seep through a possibly porous cupula. Because the approach of Van Buskirk *et al.* gives results that are largely consistent with these revised models in the low frequency and velocity regimes considered here, we use a similarly simplified geometry in the present article. It would be straightforward to extend the present work to a more complicated (but realistic) three-dimensional model of the semicircular canal.

III. MECHANICS OF THE SEMICIRCULAR CANALS AND CUPULA: MODIFICATIONS TO INCLUDE OTOCONIA

In this section, we derive a simplified model that includes the physics of settling otoconia and the processing of a velocity storage mechanism in order to quantitatively capture the essential characteristics of canalithiasis, without requiring a detailed numerical investigation. We derive an expression for the long-range pressure field exerted on the cupula by a sedimenting particle, which yields a geometric pressure amplification and a mechanism for latency. These findings confirm the feasibility of the canalithiasis mechanism for BPPV.

Four components are necessary in the analysis. In section III A, we derive an equation for the volumetric cupular displacement V_c to an externally-applied transcupular pressure difference ΔP_c . In section III B, we derive an expression for the fluid pressure field set up by a settling particle of a given size, density, and position, giving the pressure difference ΔP_c that drives the cupula. Third, the particle's settling velocity is calculated in section III C, accounting primarily for Stokes drag, but examining hydrodynamic interactions with channel walls and the effect of background endolymph flow. These three elements are sufficient to characterize the impact of a sedimenting particle on the mechanical response of the cupula, which is assumed to determine the neural signal fired. Finally, section III D incorporates the velocity storage mechanism that is assumed to process this neural signal and lengthen the (measurable) nystagmus time scale beyond the cupular time scale.

A. Physical model for flow in the semicircular canals

Throughout this study, we neglect fluid inertia, whose influence over cupular dynamics occurs on millisecond time scales, because the state of the fluid, cupula, and otoconium all change on significantly longer time scales. Without inertia, the cupular membrane obeys a simple balance of pressures, in which three terms are important. A cupular membrane that is distorted to displace a volume V_c exerts an elastic restoring force via a pressure difference $\Delta P = -KV_c$ across the membrane. (Here we choose $\Delta P = P_u - P_a$ to represent the difference in pressure between the utricular side and the ampullar side of the cupula, and V_c to be positive when the cupula is displaced into the ampulla.) Second, in order for the cupular displacement to change in time, it must force the equivalent fluid volume through the semicircular canal, requiring a pressure drop $\Delta P = -\gamma \dot{V}_c$, where γ represents viscous resistance and will be calculated shortly. The last term to enter the pressure balance is an externally applied pressure difference ΔP_c , which in our case is given by the fluid pressure set up by a settling otoconium. These three pressures balance, giving an equation for cupular displacement

$$-KV_c - \gamma \dot{V}_c + \Delta P_c(t) = 0, \quad (5)$$

replicating Steinhause's formula (2) without inertia.

Because the fluid response is taken to be quasi-steady, we can derive the viscous resistance coefficient γ in a straightforward manner. Fluid in a straight channel of length L and circular cross-section of radius b , subject to an applied pressure difference ΔP , moves with a parabolic velocity profile [22],

$$\mathbf{u}(r) = \frac{\Delta P}{4\mu L} (b^2 - r^2) \mathbf{e}_{||}, \quad (6)$$

directed along the cylinder axis $\mathbf{e}_{||}$, with flow rate $\dot{V}_c = \pi b^4 \Delta P / 8\mu L$. This provides the desired relation between pressure drop and flow rate, giving

$$\gamma = \frac{8\mu L}{\pi b^4}. \quad (7)$$

This result can be expected to provide a very good approximation for the low-Reynolds-number flow in the slightly curved canal duct and slowly-varying geometries of interest here, and several simplifying approximations can be made. We approximate the viscous resistance in the canal as occurring in the duct alone, since the pressure drop $\Delta P_{u,a} \sim b_c^4 / \beta_u$ along the utricle and ampulla is smaller than that along the duct $\Delta P_d \sim b_d^4 / \beta_d$ by approximately 10^{-3} . Furthermore, we approximate the channel as locally straight, because the radius of curvature of the channel R is large compared to the duct radius, introducing errors of magnitude $\mathcal{O}(b_d/R) \approx 0.05$ in the axial flow and $\mathcal{O}(b_d^2/R^2) \approx 10^{-3}$ in the flow rate [22]. Finally, although the channel radius is not constant, it typically varies slowly. With these approximations, the viscous resistance coefficient for the semicircular canals (equation 7) is given by

$$\gamma = \frac{8\mu\beta_d R}{\pi b_d^4}. \quad (8)$$

The cupular displacement V_c that results from an applied pressure $\Delta P_c(t)$ is given by the solution of equation (5),

$$V_c(t) = \frac{1}{\gamma} \int_{-\infty}^t \Delta P_c(t') e^{-(t-t')/\tau_c} dt', \quad (9)$$

where τ_c is time scale for cupular relaxation,

$$\tau_c = \frac{\gamma}{K} \equiv \frac{8\mu\beta_d R}{\pi b_d^4 K}, \quad (10)$$

as found by Van Buskirk *et al.* [10].

B. Pressure drop exerted by sedimenting otoconia

The time-dependent pressure $\Delta P_c(t)$ in equation (9) is provided by the stress field set up by a settling otoconium, which we model as a sphere of radius $a \ll b_d$ and density ρ_o settling through the fluid due to gravity \mathbf{g} . In viscous (low Reynolds number) fluid flows, the fluid velocity field around a translating particle is insensitive to the detailed shape or size of the particle outside of the immediate vicinity of the particle. In fact, the long-range fluid flow depends only on the total force exerted by the particle. Therefore, we can approximate the fluid flow due to the particle as that of an equivalent ‘point force,’ since $a \lesssim b_d/15$ even in the narrowest part of the curved duct.

In Appendix A, we demonstrate that the difference in pressure between the fluid in front and behind a small particle settling in a (possibly curved) circular cylinder of local radius $W(s)$ is given by

$$\Delta P = 2 \frac{\mathbf{f} \cdot \mathbf{e}_{||}}{\pi W(s_p)^2} \left(1 - \frac{r_p^2}{W(s_p)^2} \right), \quad (11)$$

which is the hydrodynamically correct analog of House and Honrubia’s equation (1). Here $\mathbf{e}_{||}$ points along the (local) cylinder axis, s_p measures the distance along the centerline of the cylinder, r_p measures the radial distance of the particle from the centerline of the canal, and \mathbf{f} is the net force exerted by the particle, given by

$$\mathbf{f} = \frac{4}{3} \pi a^3 \Delta \rho \mathbf{g}, \quad (12)$$

where $\Delta \rho = \rho_o - \rho$ is the density difference between the otoconium and the endolymph. Equation (11) was originally derived for a straight circular cylinder [23], but the physics of low-Reynolds-number flows allows it to be applied, as a first approximation, for channels whose geometry (*e.g.* radius or orientation) vary slowly. Due to the closed geometry of the semicircular canals, the pressure difference ΔP set up by the flow due to the settling sphere is exerted across the cupula, so that the forcing $\Delta P_c(t)$ in (9) is given by equations (11) and (12).

Four significant features emerge from equation (11). First, the transcupular pressure is indeed inversely proportional to the (local) cross-sectional area of the channel, as assumed by House and Honrubia[8]. This results in an amplification of ΔP_c when the particle falls into a narrowing channel. Second, the component of the force perpendicular to the channel axis gives no pressure drop, as was assumed by House and Honrubia. Third, the transcupular pressure decreases as particles approach the side walls—a significant feature for canalithiasis that is absent from House and Honrubia’s formula. Fourth, (11) is six times larger than House and Honrubia’s expression.

The radial and axial positions (r_p, s_p) of the otoconium determine the pressure ΔP_c exerted on the cupula via (11), to which the cupula responds via (9). Particle motion affects the pressure exerted on the cupula in two ways: (i) When otoconia fall from the ampulla (radius $W(s_p) = b_c$) into the narrow duct (radius $W(s_p) = b_d$), the pressure they exert is amplified by a factor $b_c^2/b_d^2 \sim 18$; and (ii) an otoconium falling straight down approaches the side of the duct due to the duct’s curvature (see Figure 1), reducing the net force in equation (11) both due to the factor $(1 - r_p^2/W(s_p)^2)$ and to the reduced force projection $\mathbf{g} \cdot \mathbf{e}_{||}$.

C. Sedimentation velocity of otoconia

Here we give an approximate calculation of the sedimentation velocity of an otoconium, considering two corrections to the standard Stokes settling velocity: hydrodynamic interactions with the walls and advection with the background flow. The advection velocity of the particle is shown to be about a thousand times smaller than its Stokes settling velocity and is thus neglected. Hydrodynamic interactions are typically small in the bulk of the channel, yet become significant when the particle nears the channel walls.

Since the particle is small compared to the size of the channel, a good first approximation to its settling speed is given simply by Stokes’ formula [22]

$$U_s = \frac{2\Delta \rho a^2 g}{9\mu} \approx 0.2 \text{ mm/s}, \quad (13)$$

using values from Table I.

We first consider the influence of the background velocity of the endolymph, which is set into motion by the displaced cupula. A cupula displacing a volume per unit time \dot{V}_c sets up a parabolic flow in the duct (equation 6), whose maximum velocity v_{\max}^e is twice its average, so that

$$v_{\max}^e = \frac{2\dot{V}_c}{\pi b_d^2}. \quad (14)$$

From the simulations discussed below (e.g. in Figure 3), we estimate a cupular volumetric displacement rate of order $\dot{V}_c \lesssim 10 \text{ pL/s}$, giving a maximum endolymph velocity in the duct of order $v_{\max}^e \lesssim 0.3 \mu\text{m/s}$, which is smaller than the Stokes settling velocity (13) by a factor of approximately 10^3 . Therefore, throughout this work, we neglect any particle advection by this background endolymph flow.

It is straightforward to incorporate previously calculated hydrodynamic interactions [24, 25] between the particle and the walls of an enclosing cylinder. Appendix B presents a description of our account of these hydrodynamic interactions. We list here the most significant features: 1) Hydrodynamic interactions are largely insignificant away from channel walls — corrections to settling velocities for particles in cylindrical channels of radius W have the form [25] $U \approx U_s [1 - (a/W)f(r_p/W)]$, where $a/W \lesssim 1/25$, representing a 1-10% correction. 2) Hydrodynamic interactions become important only as the particle gets very close to the wall, where the gap δ between the sphere and the wall becomes comparable with the particle radius a . When $\delta \ll a$, the velocity of a sphere parallel to a wall, U_{\parallel} , decreases logarithmically [24], via

$$U_{\parallel} \approx \frac{U_s}{\log(\delta/a)}, \quad (15)$$

whereas the velocity of a sphere forced perpendicular to a wall, $U_{\perp} \approx U_s \delta/a$, decreases linearly with δ , so that δ decays exponentially in time. When $\delta \ll a$, however, the particle is very close to the walls and so exerts a vanishingly small force upon the cupula. Consequently, the effect that near-wall hydrodynamic interactions have on modifying equation (11) for ΔP_c are insignificant for cupular dynamics, since ΔP_c is itself very small. 3) When the particle is so close to the wall that $\delta \sim a$, many of the approximations we use do not hold: the non-spherical shape of real otoconia may play a significant role for otoconia very close to canal walls, and canal walls are coated with a *membraneous* duct [9] rather than a smooth solid one. It seems likely that otoconia must slide along the duct walls, for otherwise the therapeutic maneuvers would be geometrically impossible. Because of our uncertainty about the actual shape of the particles and the nature of the otoconia/wall interactions when the two are extremely close, we have introduced an arbitrary cutoff distance $\delta_c \approx 1 \mu\text{m}$ in the numerical simulations shown below. When the gap between the particle and the channel wall is within this distance δ_c , the particle is assumed to slide with the velocity given by equation (15) with $\delta = \delta_c$. The resulting motion is insensitive to the particular value of δ_c : choosing δ_c to be ten times smaller would only slow the ‘sliding’ velocity by a factor of $\log(10) \approx 2.3$ when the particle is close to the boundary.

D. Velocity storage as a model of neural processing

Our treatment thus far has concerned only the mechanical response of the system. Signal processing is believed to occur in the brain stem in a process called velocity storage [11, 12]. While velocity storage does not affect the mechanical response of the semicircular canals, it does affect the (measurable) nystagmus response, denoted \dot{E} (since it refers to time-dependent eye movement), and we therefore include it in the present work. The effect of velocity storage is to lengthen the long time constant of the horizontal semicircular canal $\tau_c \approx 4.2$ seconds [15] to a longer time scale $\tau_v \approx 16 - 21$ seconds [15, 26], which improves the performance of the canals for angular rate sensing, extending their bandwidth to lower frequencies. The velocity storage mechanism is typically described in Laplace transform space (indicated by tildes) using a transfer function [11, 12]

$$\frac{\tilde{\dot{E}}(s)}{\tilde{\Omega}_c(s)} = \frac{1 + s\tau_c}{1 + s\tau_v}. \quad (16)$$

where Ω_c is the angular velocity perceived by the canal, according to cupular displacement (equation 4). Combining equation (16) with the Laplace transform of equation (5), we arrive at an expression for nystagmus as a function of transcupular pressure,

$$\dot{E}(t) = \frac{\lambda^4}{32\rho(\beta_u + \beta_d)R^2} \int_{-\infty}^t \Delta P_c(t') e^{-(t-t')/\tau_v} dt'. \quad (17)$$

This expression allows us to translate the mechanical effect of a sedimenting particle into an equivalent sensation of motion, which is directly measurable as an eye movement.

As stated above, we have assumed that the well-known velocity storage mechanism, which operates in the lateral canal, is also effective for the posterior canal. However, in the absence of any experimental evidence — on humans or animals — to guide us, we have assumed the same velocity storage mechanism exists in the posterior and lateral canals.

IV. SIMULATIONS OF CANALITHIASIS

We model canalithiasis as follows: numerically place an otoconium below the cupula and follow its motion in time as it enters the duct and intersects the channel wall. The fluid pressure $\Delta P_c(t)$ exerted on the cupula are calculated, and the cupular deflection and nystagmus are determined by numerically integrating equations (9-12) and (17). Two examples are considered: Section IV A examines the cupular response to a particle settling in a circular cylindrical channel which tapers from one constant radius to another. While the straight channel is physically unrealistic, this simulation is instructive in highlighting the pressure-amplification mechanism described by equation (11). Section IV B presents a simulation of a attack of BPPV for an average-sized otoconium starting just below the cupula in a model canal whose geometry (Figure 1) mimics the semicircular canals in that (i) it tapers from the ampulla to the duct in approximately the same manner, and (ii) the canal curves with a major radius taken from measurements [9]. Such features of BPPV as latency, strength and duration are presented.

A. Cupular response to a particle settling in a straight, tapering channel

A straight, tapering channel provides a particulary simple illustration of the pressure amplification provided by a narrowing channel, which is expected to be a significant dynamical feature accompanying sedimentation of an otoconium, and highlights the hydrodynamic explanation for latency.

We consider a particle of radius a that settles along the midline of a straight vertical channel of varying radius $W(s_p)$

$$W(s_p) = \frac{b_c + b_d}{2} - \frac{(b_c - b_d)}{2} \tanh\left(\frac{s - s_0}{R\delta}\right), \quad (18)$$

so that $W(-\infty) = b_c$ and $W(\infty) = b_d$ (see the profile sketched in Figure 2). The specific functional form in equation (18) has been chosen for convenience but has the feature of narrowing from b_c to b_d over a distance $R\delta$, which captures one significant geometric feature of the semicircular canal (Figure 1). Neglecting hydrodynamic interactions with the wall, the sphere settles at the Stokes settling velocity, so that its axial position is given by $s_p(t) = U_s t$, where U_s is given by equation (13). Viscous resistance to the settling sphere sets up a time-dependent pressure drop on the cupula found by combining equations (11) and (18),

$$\Delta P_c(t) = \frac{32a^3\Delta\rho g}{3\{(b_c + b_d) - (b_c - b_d)\tanh[(U_s t - s_0)/R\delta]\}^2}, \quad (19)$$

which is plotted in Figure 2. As the particle settles through the narrowing portion of the channel, the pressure it exerts on the cupula increases by a factor $b_c^2/b_d^2 \approx 18$, and asymptotically approaches a constant value $\Delta P_c^\infty = 8a^3\Delta\rho g/3b_d^2$. The cupular displacement is then given by equation (9) and is shown in Figure 2 as well. After many time constants τ_c , the cupular displacement asymptotically approaches its limiting value

$$V_c^\infty = \frac{\Delta P_c^\infty \tau_c}{\gamma} = \frac{8a^3\Delta\rho g}{3Kb_d^2} \approx 57\text{pL}, \quad (20)$$

where we have evaluated V_c^∞ using the typical values reported in Table I. The nystagmus response $\dot{E}(t)$, calculated using equation (17), is also plotted in Figure 2 and responds over the longer time scale τ_v .

This simulation is representative of basic hydrodynamic processes and corresponding cupular responses, but is nevertheless unrealistic, as the real semicircular canal is curved and the forcing is truncated when the otoconium hits the wall. It does, however, clearly demonstrate the pressure-amplification effect of the tapering canal. The effect of canal curvature in a more realistic model geometry is considered next.

B. Two-part toroidal model for semicircular canal

The above section demonstrated the force-amplification effect provided by a tapering channel (as would be found by an otoconium falling from the ampulla into the duct). In this section, we consider a geometry which more closely resembles a semicircular canal — a two-part torus with major radius R , with a thick ampulla region (of radius b_c) and a thin duct region (of radius b_d and angular span β_d), as shown in Figure 1. For analytical convenience, we represent

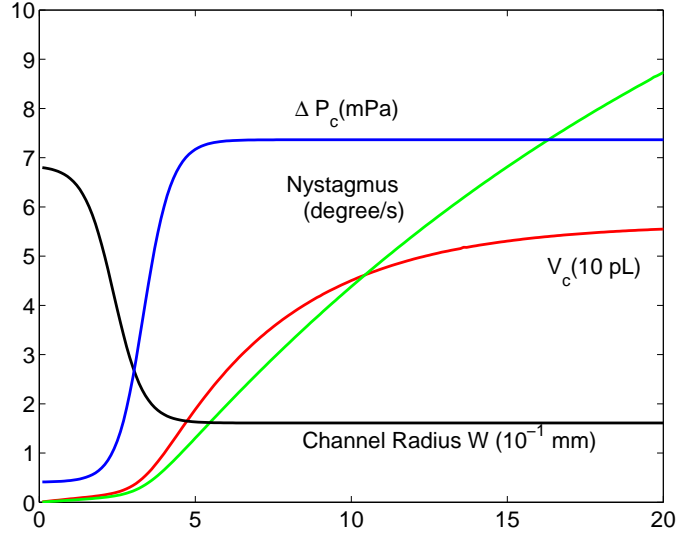


FIG. 2: Cupular pressure $\Delta P_c(t)$, displacement $V_c(t)$ and nystagmus response $\dot{E}(t)$ as an otoconium falls through a straight, tapering channel (whose profile is also indicated). The settling otoconium sets up a pressure field that is small when the otoconium is in the wide part of the channel ($t < 3$ seconds) and jumps by a factor $b_c^2/b_d^2 \approx 18$ when the otoconium enters the narrow part of the channel. Correspondingly, the cupular displacement increases slowly while the force is small (≈ 3 seconds), then increases over a timescale τ_c to the large, constant force as the otoconium falls through the duct. The nystagmus response is similar, but increases over a much larger time τ_v . Several seconds of ‘latency’ can be seen as the particle settles through the wide part of the channel, after which the force-amplifying effect of the narrowing canal sets in. Geometrical and physical parameters are given in Table I.

the inner and outer radii of the canal as functions of angle ($0 < \theta \leq 2\pi$),

$$R_{\text{out}} = R + b_d \quad \text{and} \quad R_{\text{in}} = R - \left[A + B \tanh \left(\frac{\theta - \theta_1}{\delta} \right) \right], \quad (21)$$

where $A = 2b_c + b_d$ and $B = 2b_c - b_d$. The canal narrows from radius b_c in the ampulla to b_d in the duct (see Figure 3a). We define the cupula to be located at $\theta = 0$, and the narrowing occurs roughly over an angle 2δ , centered around θ_1 . Examining the measurements of Curthoys and Oman [9], we choose $\theta_1 = 0.5\pi$ and $\delta = 0.03\pi$, and $b_c = 0.68$ mm and $b_d = 0.16$ mm so that the circular channels employed here have cross-sectional areas equal to the roughly elliptical channels they measured. The pressure amplification described in Section IV A occurs in this more realistic geometry as well; furthermore, the curvature of the duct (with radius of curvature R) leads the otoconium to fall away from the central axis of the duct, leading to a diminished pressure according to equation (11).

Figure 3a shows three otoconium trajectories (A, B, C) in the early time of an attack of BPPV when an otoconium falls from the cupula onto the curved tapering region. Figure 3b shows the cupular displacement, pressure, and nystagmus response corresponding to each trajectory. Dark dots are located every two seconds to make the time-dependence along the trajectory more evident. Three distinct features can be seen in trajectory B: 1) an initial period (approximately 5 seconds) in which the cupular displacement grows slowly, which occurs while the otoconium is in the ampulla, 2) an intermediate period (approximately 4 seconds) where the cupular displacement increases rapidly, when the otoconium has entered the narrow duct, yet not hit the wall, and 3) a final period where the cupular displacement decays with time constant τ_c , after the otoconium has hit the wall and no longer exerts a pressure on the cupula. From the trajectories of the particles, it is evident that hydrodynamic interactions between the particles and the wall are negligible until the particle is very close to the wall. Because the resistance to sliding along the wall decreases only logarithmically with the separation distance (equation (15)), and because we have instituted a minimum particle-wall separation δ_c , the particle continues to move significant distances even when close to the wall (figure 3a).

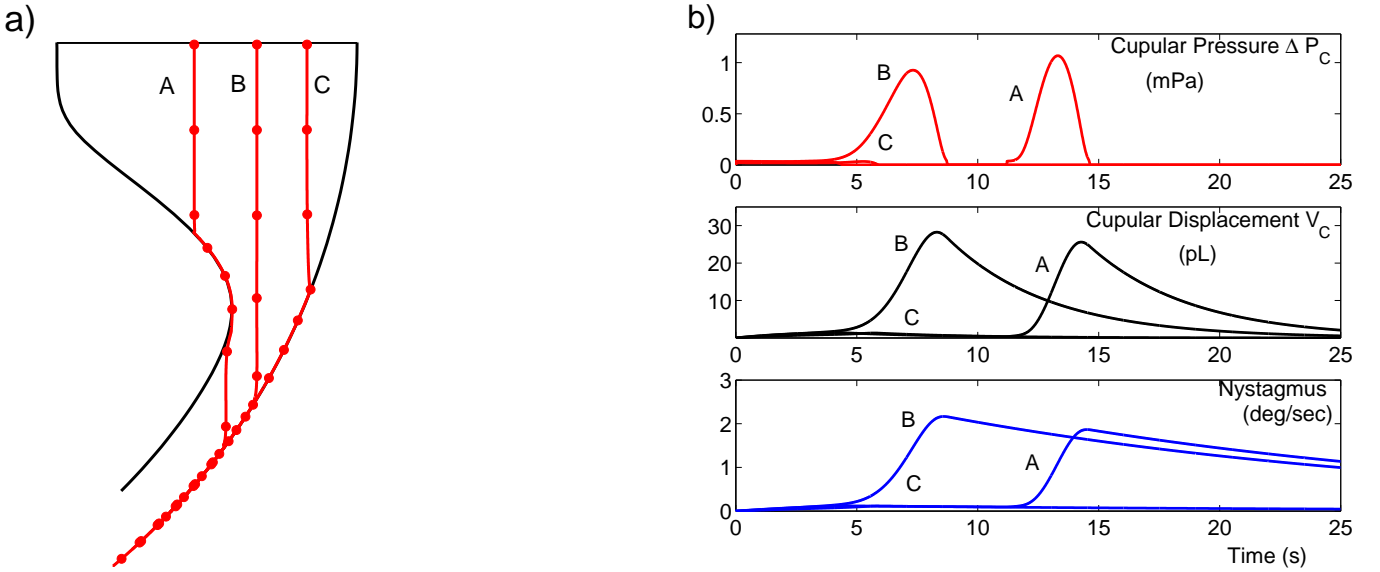


FIG. 3: Simulated canalithiasis episodes occurring when otoconia started at different radial positions just below the cupula fall through a tapering toroidal channel. a) Otoconia trajectories, with dots to indicate the location each otoconium every 2 seconds. b) Results for (i) the pressure exerted on the cupula for the three trajectories, (ii) the cupular displacement for each of the three trajectories , and (iii) the nystagmus response, reflecting the sensed rotation velocity. The largest cupular displacement occurs when the otoconium enters the narrow part of the canal, hydrodynamically amplifying the pressure it exerts by a factor of up to 36 times the naive estimate of F_g/A_c (which would occur during cupulolithiasis). This occurs with a 6-13 second latency for trajectories A and B, and never occurs for trajectory C, which hits the wall before entering the duct.

V. INFLUENCE OF OTOCONIUM SIZE UPON CUPULAR PRESSURE AND DISPLACEMENT

Otoconia have been found in a range of sizes, typically between $0.5-15 \mu\text{m}$ [14]. In this section, we provide some guidelines for the influence of otoconium size on the responses illustrated in the previous sections. We showed above that hydrodynamic interactions with the walls do little to an otoconium's trajectory until it comes very close to the wall, at which time the pressure field exerted at the cupula is negligible. Therefore, the dependence of the cupular pressure $\Delta P_c(t)$ (and its time dependence) upon particle size a can be predicted, from which cupular and nystagmus response follow.

An otoconium sets up a pressure field proportional to its mass ($\Delta P \sim a^3$), but since its settling velocity varies with a^2 , this pressure field is set up for a time which varies with a^{-2} . Thus the peak cupular displacement and nystagmus increase linearly with particle size a , so long as the particles do not settle longer than τ_c or τ_v , respectively. Figure 4 shows a series of simulations where particles of varying radius a fell along trajectory B of figure 3, and the maximum cupular displacement and nystagmus increase linearly with particle size a for particles larger than a few microns.

A large repertoire of eye movement responses are possible for the various sizes, trajectories, and collective behavior of otoconia. Multiple otoconia may be clumped or dispersed. A clumped group of N otoconia would behave like a single larger particle (of radius $a' \approx N^{1/3}a$), giving a maximum cupular displacement which is approximately $N^{1/3}$ times larger than for a single otoconium. On the other hand, a group of N dispersed otoconia settling independently would give a total cupular displacement and nystagmus approximately N times greater than for a single otoconium.

Peak nystagmus typically decreases with repeated head maneuvers [1], a fact which is typically attributed to the breaking and dispersion of particle clumps and/or particle margination. The dispersion explanation of fatigability seems at odds with the above results, which suggests that particle dispersion would increase the peak nystagmus: the pressure exerted by each independently-moving particle would add linearly, giving the same total pressure, but exerted over a longer time than a faster-moving particle clump.

We propose several mechanisms to reconcile these pictures: 1) Particle margination: repeated maneuvers presumably break up clumps and disperse the particles, which when isolated might adhere to the membranous canal walls. 2) If a particle clump is so large that it occupies a significant fraction of the duct, it would exert a substantially larger transcupular pressure, and would move significantly more slowly, than individual particles and result in substantially greater nystagmus. The breakup of such a large clump would result in a lesser nystagmus response. Whether such large clumps exist or are reasonable is not known. 3) The response of dispersed particles could result in weaker

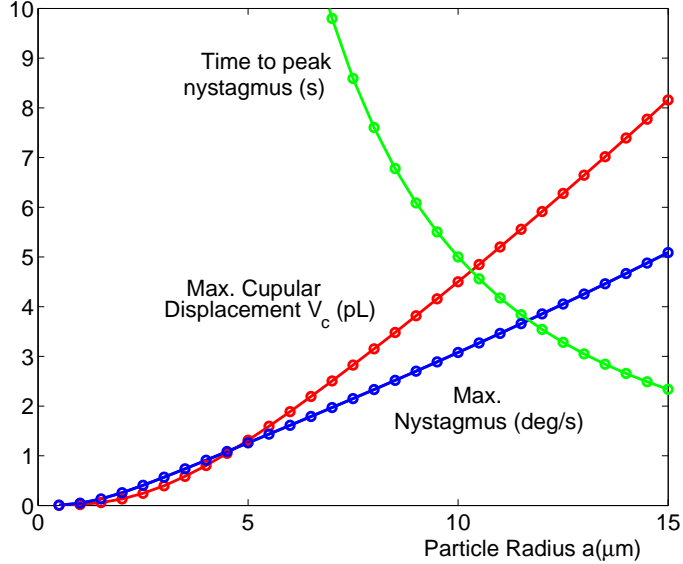


FIG. 4: Simulations for particles of different radii, all started on trajectory B in the model semicircular canal geometry of Figure 3. The maximum nystagmus and cupular displacement are plotted, and increase linearly with particle size for particles larger than a few microns. The time at which peak nystagmus occurs is plotted, and varies in proportion to $1/a^2$.

nystagmus than a single clumped stone if the dispersed particles follow different trajectories. As shown in figure 3, the nystagmus response is sensitive to the trajectory a particle takes, affecting both transcupular pressure and the time trajectory.

VI. CUPULOLITHIASIS

Most of this article has concerned the canalithiasis mechanism for BPPV. An alternate hypothesis for BPPV is cupulolithiasis, in which otoconia are physically attached to the cupula, causing it to distort when the head is turned. In cupulolithiasis, the pressure exerted by a head suddenly turned would be constant. The maximum possible cupular displacement and nystagmus would occur if the head were tilted and held in a position such that gravity acts normal to the cupula. In this ‘worst-case’ scenario, the transcupular pressure is given by $\Delta P_c = (4\pi/3)a^3\Delta\rho g/A_c$, and the corresponding cupular displacement is given by

$$V_c(t) = \frac{F_g}{KA_c} \left(1 - e^{-t/\tau_c}\right), \quad (22)$$

with a nystagmus response

$$\dot{E}(t) = \frac{\pi\lambda^4 a^3 \Delta\rho g}{24\rho(\beta_u + \beta_d)R^2 A_c} \tau_v \left(1 - e^{-t/\tau_v}\right) \approx 0.6^\circ/s \left(1 - e^{-t/\tau_v}\right). \quad (23)$$

Thus even if the head were tilted and held in place indefinitely, the nystagmus response for an average otoconium attached to the cupula would approach a constant $\dot{E} \approx 0.6^\circ/s$. The cupular displacement ($V_c \rightarrow F_g/KA_c \approx 2 \text{ pL}$) is an order of magnitude smaller than that which would occur due to an identical otoconium sedimenting through the narrowing duct under the canalithiasis mechanism, and the maximum possible nystagmus is 3-4 times weaker than that for canalithiasis. The nystagmus due to a single, average otoconium is below the detection threshold, meaning that multiple and/or larger otoconia are required for cupulolithiasis. Furthermore, one would typically expect significantly weaker nystagmus than (23), since the head would typically not be held in the optimal orientation required, for the 20-60 seconds necessary to achieve this maximal response.

VII. CONCLUSIONS

In this paper we have developed a mathematical model for the transcupular pressure amplification generated by a sedimenting particle in a geometry characteristic of the semicircular canals. The hydrodynamic aspects of the motion are treated within the constraints of the low-Reynolds-number-flow representative of these systems and the model is coupled to the velocity storage mechanism representative of neural signal processing in the brain stem.

Our results are qualitatively consistent with the recent study of House and Honrubia, though should be considered quantitatively more accurate since the basic hydrodynamics are explicitly treated. House and Honrubia performed a one-dimensional simulation (with otoconia constrained to fall along the canal centerline) using (1) for transcupular pressure, and found that an otoconium mass $m_H \approx 0.087\mu\text{g}$ (or 18 otoconia of radius $7.5\mu\text{m}$) would be required to achieve a (measured) peak nystagmus of $\dot{E} \approx 42^\circ/\text{s}$. For comparison, an analogous one-dimensional simulation using (11), the pressure drop we derived by solving the Stokes equations, would require about three otoconia ($0.014\mu\text{g}$). More realistically, however, otoconium fall to the side walls due to duct curvature, which diminishes the transcupular pressure. From figure 3b, one average-sized otoconium can cause a nystagmus of approximately $2^\circ/\text{s}$, so that approximately 20 otoconia, or $0.1\mu\text{g}$, would be required to account for the same measured nystagmus. That the two models give similar results is fortuitous – the near cancellation of two effects.

The model demonstrates that sedimentation from the wide region near the cupula to the narrow region representative of most of the semicircular canal takes about 5-6 seconds for a typical case with an otoconium of average size, and that the entry into the narrowing duct is accompanied by a pressure amplification of a factor of approximately $b_c^2/b_d^2 \approx 18$ relative to the pressure exerted while the otoconium is in the ampulla. Conversely, if an otoconium moves from the narrow duct into the wider utricle, as is assumed to occur during therapeutic maneuvers, the pressure it exerts on the cupula drops significantly. This scenario provides a possible resolution to an issue raised by Buckingham [7], who suggested that otoconia moved into the utricular region during therapeutic maneuvers should still exert a fluid pressure on the cupula and cause BPPV. This conjecture is at odds with the success of the maneuvers, and led Buckingham to question the feasibility of canalithiasis. However, the pressure-amplification mechanism discussed in this article results in a pressure *reduction* in the utricle, so that the transcupular pressure set up by an otoconium settling in the utricle may be small enough to escape detection.

The results of the hydrodynamic modelling reported here are consistent with the observed latency of BPPV, and provide a possible mechanism, as was also suggested by House and Honrubia. Furthermore, the pressure exerted by a sedimenting otoconium (in canalithiasis) is amplified by a factor of up to $2b_c^2/b_d^2 \approx 36$ over that of a particle attached to the cupula (as in cupulolithiasis). An average otoconium of radius $7.5\mu\text{m}$ exerts a pressure on the cupula which induces an equivalent step increase in angular velocity in the range of $2^\circ/\text{s}$, approximately the threshold for sensation. The stronger sensations experienced during real attacks of BPPV could result from larger or multiple otoconia.

APPENDIX A: AN APPLICATION OF THE RECIPROCAL THEOREM FOR A POINT FORCE IN A TUBE OF SLOWLY VARYING RADIUS

In this appendix we use the reciprocal theorem from low-Reynolds-number hydrodynamics [22] to determine the pressure drop at large distances from a point force (Stokeslet) in a tube. This analysis was apparently first given by Brenner [23] for a point force in a circular cylinder and we show that the same ideas can be extended naturally to a tube of arbitrarily varying cross section and orientation.

Recall that the reciprocal theorem relates two solutions $(\mathbf{u}, \sigma, \mathbf{f})$ and $(\hat{\mathbf{u}}, \hat{\sigma}, \hat{\mathbf{f}})$ to the Stokes equations

$$\nabla \cdot \mathbf{u} = 0 \quad (\text{A1})$$

$$\nabla \cdot \sigma + \mathbf{f} = \mathbf{0}, \quad (\text{A2})$$

where σ is the stress tensor,

$$\sigma_{ij} = -P\delta_{ij} + \frac{\mu}{2} \left(\frac{\partial u_i}{\partial x_j} + \frac{\partial u_j}{\partial x_i} \right), \quad (\text{A3})$$

from which equation (A2) attains its more familiar form $\mu\nabla^2\mathbf{u} - \nabla P + \mathbf{f} = \mathbf{0}$. Here \mathbf{u} and \mathbf{f} represent, respectively, the velocity field and force per unit volume acting on the fluid. Then, within a volume V and corresponding bounding surface S , these fields are related by

$$\int_S \mathbf{n} \cdot \sigma \cdot \hat{\mathbf{u}} \, dS - \int_S \mathbf{n} \cdot \hat{\sigma} \cdot \mathbf{u} \, dS = - \int_V \mathbf{u} \cdot \hat{\mathbf{f}} \, dV + \int_V \hat{\mathbf{u}} \cdot \mathbf{f} \, dV, \quad (\text{A4})$$

where \mathbf{n} is the unit normal directed into the fluid domain from the surface. Here we take $(\mathbf{u}, \sigma, \mathbf{f})$ for fields associated with a Stokeslet inside an infinitely long tube of arbitrary cross-sectional shape and we use $(\hat{\mathbf{u}}, \hat{\sigma}, \hat{\mathbf{f}})$ for the flow caused by a uniform uniaxial pressure gradient. In this case, the volume V corresponds to the interior of the tube. For a circular pipe of uniform cross-section, the ‘hatted’ flow is simply the well-known Poiseuille flow. Now, due to the no-slip condition on the walls of the duct, the surface integrals in equation (A4) are only nonzero at the ‘ends’ of the duct, which we consider to be at a very large distance (many cylinder radii) from the point force.

We now simplify (A4) in steps. First, the pressure-driven flow contains no body forces in V , $\hat{\mathbf{f}} = \mathbf{0}$. Second, the flow due to a Stokeslet in a bounded cylindrical domain decays exponentially with axial distance from the singularity [27], so $\mathbf{u} \rightarrow \mathbf{0}$ towards the ends of the duct. Further, since \mathbf{f} corresponds to a Stokeslet of strength \mathbf{F} , then $\mathbf{f} = \mathbf{F}\delta(\mathbf{r})$, where $\delta(\mathbf{r})$ denotes the Dirac delta function, and we may evaluate the second integral on the right-hand side of (A4) as $\hat{\mathbf{u}}_s(\mathbf{x}_s) \cdot \mathbf{F}$, where $\hat{\mathbf{u}}_s(\mathbf{x}_s)$ is the pressure-driven velocity field at the location \mathbf{x}_s of the Stokeslet.

Since the ‘ends’ of the cylinder are considered far from the Stokeslet where $\mathbf{u} \rightarrow \mathbf{0}$, then the corresponding stress field is simply a pressure that remains constant across each ‘end’ section. If we denote the difference in pressures between the two ‘ends’ as Δp , then the first term on the left-hand side of (1) reduces to $\hat{Q}\Delta p$, where \hat{Q} is the volume flux due to the pressure-driven flow. Combining the above results gives

$$\Delta p = \frac{\mathbf{F} \cdot \hat{\mathbf{u}}_s}{\hat{Q}}. \quad (\text{A5})$$

This holds for a tube of arbitrarily varying cross-section and orientation.

Finally, we invoke the lubrication approximation, which provides that for a circular tube of slowly varying radius $W(s)$ the flow velocity is given by

$$\hat{\mathbf{u}}_s = U_0 \left(1 - \frac{r_s^2}{W(s)^2} \right) \mathbf{e}_{||}, \quad (\text{A6})$$

with corresponding flow rate

$$\hat{Q} = \frac{\pi W(s)^2 U_0}{2}. \quad (\text{A7})$$

Using (A5), we find the Stokeslet sets up a pressure difference

$$\Delta p = \frac{2\mathbf{F} \cdot \mathbf{e}_{||}}{\pi W(s)^2} \left(1 - \frac{r_s^2}{W(s)^2} \right). \quad (\text{A8})$$

APPENDIX B: SUMMARY OF RESULTS FOR A SPHERE SETTLING IN A CIRCULAR CYLINDER

This appendix summarizes several results for the hydrodynamic influence of the cylinder walls upon the motion of a small sedimenting particle. Our motivation for including this appendix is twofold: 1) to explain how hydrodynamic coupling between the wall and the particle can be treated in a reasonably straightforward yet accurate manner, and 2) to demonstrate that this hydrodynamic coupling is largely unimportant in modelling the sedimentation of small particles in the semicircular canals. In regard to the second point, the walls only exert a significant influence upon the motion of a sedimenting particle when the particle is very close to the wall. In this limit, however, the fluid pressure on the cupula due to the sedimenting particle (given by equation 11) is exceedingly small. Therefore, wall-particle interactions are typically not significant for modelling cupular displacement, but are important when the trajectories of the particles are themselves of interest.

A simple expression for the sedimentation velocity of a sphere in a geometry as complicated as that of the semicircular canals is unavailable. However, because the radius of curvature of the torus R is much larger than the radius of the canals b , we approximate the canals as straight circular cylinders, which involves errors of order $\mathcal{O}(b/R)$. Even for this comparatively simple geometry, no uniformly valid expression is known for the motion of a sphere through a viscous fluid in a circular cylindrical container. Rather, numerical and asymptotic formulae have been derived in various limits. In this appendix, we summarize several results, which we use in our simulation of canalithiasis.

We consider a small spherical particle of radius a , with externally applied force $\mathbf{f} = F_z \hat{\mathbf{z}} + F_r \hat{\mathbf{r}}$, located at radius r_p in a circular cylinder of radius b . Following the notation of Hirschfeld, Brenner and Falade [25], we introduce two dimensionless parameters, $\beta = r_p/b$ and $\kappa = a/b$ to characterize the system. The parameter β indicates the dimensionless radial position of the particle, and κ gives a dimensionless particle radius.

In modelling the sedimentation of otoconia in the semicircular canals, we are concerned with the motion of particles that are small with respect to the size of the cylinder, and thus restrict our attention to the regime $\kappa \ll 1$. Within

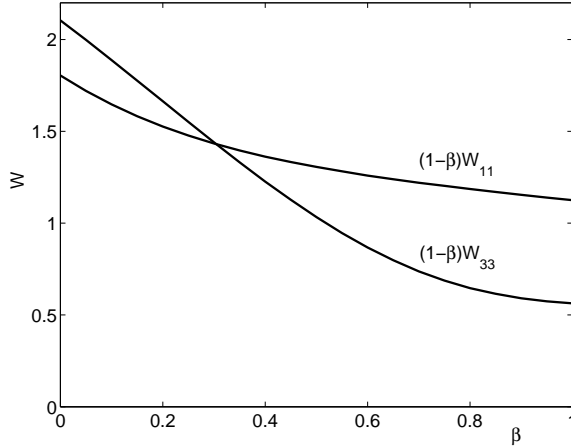


FIG. 5: (From [25], Table 2.) Numerical factors for equations (B1) - (B1) giving corrections to the velocity of a sphere in an infinite, straight, circular cylinder which is forced radially (W_{11}) or axially (W_{33}). Here $\beta = r_p/b$ is a measure of the sphere's fractional distance to the wall. Both W_{11} and W_{33} diverge like $(1 - \beta)^{-1}$ as the sphere nears the wall, which is the reason we have plotted $(1 - \beta)W_{11}$ and $(1 - \beta)W_{33}$.

this limit, there are two primary regimes: 1) $1 - \beta \gg \kappa$, where the distance from the particle to the wall is large compared to the particle size, and 2) $1 - \beta \sim \kappa$, where the particle is close to the wall.

When the distance between the sphere and the cylinder walls ($b - r_p$) is large compared to the particle radius a , a method of reflections can be used to perturbatively calculate the influence of the wall upon the motion of the sphere. Hirschfeld, Brenner and Falade [25] give results accurate to $\mathcal{O}(\kappa^2)$ for the velocity of a sedimenting sphere; we here quote results only to $\mathcal{O}(\kappa)$:

$$U_{\perp}(r_p \gg a) = \frac{F_r}{6\pi\mu a} (1 - \kappa W_{11}) \quad \text{and} \quad U_{\parallel}(r_p \gg a) = \frac{F_z}{6\pi\mu a} (1 - \kappa W_{33}), \quad (\text{B1})$$

where W_{11} and W_{33} are dimensionless functions, numerically computed in [25] and plotted in Figure 5.

A different behavior is found when the sphere is close to the wall, and the gap $\delta = b - r_p$ is smaller than a , and correspondingly the cylinder radius is much larger than both the gap and the sphere. The leading-order approximation to the settling speed of the sphere can be found by treating the cylinder wall as locally planar. Goldman, Cox and Brenner [24] studied this system using a lubrication approach, finding

$$U_{\parallel} \approx \frac{2F_{\parallel}}{6\pi\mu a} \left[\frac{\ln(\delta/a) - 0.9543}{\{\ln(\delta/a)\}^2 - 4.325 \ln(\delta/a) + 1.591} \right], \quad (\text{B2})$$

as a leading-order asymptotic formula for the velocity of a sphere parallel to a wall. The velocity parallel to the wall thus decays very slowly, with an approximately $\sim 1/\ln(\delta)$ correction. Motion perpendicular to a planar wall due to F_{\perp} can be found using the lubrication approximation in the limit $\delta \ll a$, giving

$$U_{\perp} = \frac{F_{\perp}\delta}{12\pi\mu a^2\lambda_{\perp}}, \quad (\text{B3})$$

so that a sphere exponentially approaches the wall with time constant $\tau_{\perp} = 12\pi\mu a^2/F$.

[1] T. Brandt, *Vertigo: its multisensory syndromes* (Springer-Verlag, London, 1991).
[2] J. S. Oghalai, S. Manolidis, J. L. Barth, M. G. Stewart, and M. A. Jenkins, *Otolaryngol. Head Neck Surg.* **122**, 630 (2000).
[3] T. Brandt and S. Steddin, *J. Vest. Res.* **3**, 373 (1993).
[4] J. M. Epley, *Otolaryngol. Head Neck Surg.* **107**, 399 (1992).
[5] A. Semont, G. Freyss, and E. Vitte, *Adv. Otorhinolaryngol.* **42**, 290 (1998).
[6] T. Brandt and R. B. Daroff, *Arch. Otolaryngol.* **106**, 484 (1980).
[7] R. A. Buckingham, *Laryngoscope* **109**, 717 (1999).

- [8] M. G. House and V. Honrubia, *Audiol. Neurotol.* **8**, 91 (2003).
- [9] I. S. Curthoys and C. M. Oman, *Acta Otolaryngol. (Stockh)* **103**, 254 (1987).
- [10] W. C. V. Buskirk, R. G. Watts, and Y. K. Liu, *J. Fluid Mech.* **78**, 87 (1976).
- [11] D. A. Robinson, *Exp. Brain Res.* **30**, 447 (1977).
- [12] T. Raphan, V. Matsuo, and B. Cohen, *Exp. Brain Res.* **35**, 229 (1979).
- [13] J. P. Bronzino, *The Biomedical Engineering Handbook* (CRC Press, 1995).
- [14] A. Campos, *Adv. Otorhinolaryngol.* **45**, 143 (1990).
- [15] M. Dai, A. Klein, B. Cohen, and T. Raphan, *J. Vest. Res.* **9**, 293 (1999).
- [16] R. Malcolm, in *4th Symp. on Role of Vestibular Organs in Space Exploration* (U. S. Government Printing Office, N.A.S.A. SP-187, Washington, D.C., 1968).
- [17] W. Steinhausen, *Pflügers Arch. Ges. Physiol.* **232**, 500 (1933).
- [18] C. Fernandez and J. M. Goldberg, *J. Neurophysiol.* **34**, 635 (1971).
- [19] C. M. Oman, E. N. Marcus, and I. S. Curthoys, *Acta Otolaryngol. (Stockh)* **103**, 1 (1987).
- [20] R. D. Rabbitt and E. R. Damiano, *J. Fluid. Mech.* **307**, 333 (1996).
- [21] E. R. Damiano, *J. Biomed. Eng.* **121**, 449 (1999).
- [22] L. G. Leal, *Laminar Flow and Convective Transport Processes* (Butterworth-Heinemann, Boston, 1992).
- [23] H. Brenner, *Phys. Fluids* **1**, 338 (1958).
- [24] A. J. Goldman, R. G. Cox, and H. Brenner, *Chem. Eng. Sci.* **22**, 637 (1967).
- [25] B. R. Hirschfeld, H. Brenner, and A. Falade, *Physicochem. Hydrodyn.* **5**, 99 (1984).
- [26] T. C. Hain and D. S. Zee, *Ann. N. Y. Acad. Sci.* **656**, 297 (1992).
- [27] J. R. Blake, *J. Fluid Mech.* **95**, 209 (1979).